Fusion Engineering and Design 89 (2014) 2838–2844

Contents lists available at ScienceDirect

Fusion Engineering and Design

journal homepage: www.elsevier.com/locate/fusengdes

Active radiative liquid lithium divertor concept

M. Ono[a,*], M.A. Jaworski[a], R. Kaita[a], Y. Hirooka[b], D. Andruczyk[c], T.K. Gray[d], the NSTX-U Research Team

[a] Princeton Plasma Physics Laboratory, PO Box 451, Princeton, NJ 08543, USA
[b] National Institute for Fusion Science, 322-6 Oroshi, Toki, Gifu 509-5292, Japan
[c] Center for Plasma-Materials Interactions, University of Illinois, Urbana-Champaign, IL, USA
[d] Oak Ridge National Laboratory, PO Box 2008, Oak Ridge, TN 37831, USA

HIGHLIGHTS

- In this paper, we propose an active radiative liquid lithium divertor concept (ARLLD).
- We summarize a previously introduced radiative liquid lithium divertor (RLLD) concept.
- We also point out various roles liquid lithium can play in the divertor system with ARLLD complementing RLLD.
- We point out the ARLLD can play an effective first line of defense for protecting divertor PFCs.

ARTICLE INFO

Article history:
Received 2 December 2013
Received in revised form 14 May 2014
Accepted 15 May 2014
Available online 20 June 2014

Keywords:
International lithium symposium
Lithium
Divertor
Plasma–wall interactions

ABSTRACT

Developing a reactor compatible divertor has been identified as a particularly challenging technology problem for magnetic confinement fusion. Application of lithium (Li) in NSTX resulted in improved H-mode confinement, H-mode power threshold reduction, and reduction in the divertor peak heat flux while maintaining essentially Li-free core plasma operation even during H-modes. These promising Li results in NSTX and related modeling calculations motivated the radiative liquid lithium divertor (RLLD) concept [1]. In the RLLD, Li is evaporated from the liquid lithium (LL) coated divertor strike point surface due to the intense heat flux. The evaporated Li is readily ionized by the plasma due to its low ionization energy, and the poor Li particle confinement near the divertor plate enables ionized Li ions to radiate strongly, resulting in a significant reduction in the divertor heat flux. This radiative process has the desired effect of spreading the localized divertor heat load to the rest of the divertor chamber wall surfaces, facilitating divertor heat removal. The modeling results indicated that the Li radiation can be quite strong, so that only a small amount of Li (~a few mol/s) is needed to significantly reduce the divertor peak heat flux for typical reactor parameters. In this paper, we examine an active version of the RLLD, which we term ARLLD, where LL is injected in the upstream region of divertor. We find that the ARLLD has similar effectiveness in reducing the divertor heat flux as the RLLD, again requiring only a few mol/s of LL to significantly reduce the divertor peak heat flux for a reactor. An advantage of the ARLLD is that one can inject LL proactively even in a feedback mode to insure the divertor peak heat flux remains below an acceptable level, providing the first line of defense against excessive divertor heat loads which could result in damage to divertor PFCs. Moreover, the low confinement property of the divertor (i.e., <1 ms for Li particle confinement time) makes the ARLLD response fast enough to mitigate the effects of possible transient events such as large ELMs.

1. Introduction

Developing a reactor-compatible divertor system is a particularly challenging physics and technology problem for magnetic confinement fusion [2,3]. While tungsten has been identified as the most attractive solid divertor material, many challenges including surface cracking and deleterious modification of the surfaces by the plasma must be overcome to develop robust plasma facing components (PFCs) [4]. In recent DEMO divertor design studies [5–7], the steady-state heat handling capability of a tungsten-based divertor design is only about 5–10 MW/m^2, which is nearly an order of magnitude lower than the anticipated unmitigated heat flux

* Corresponding author. Tel.: +1 609 243 2105; fax: +1 609 243 2222.
E-mail address: mono@pppl.gov (M. Ono).

http://dx.doi.org/10.1016/j.fusengdes.2014.05.008
0920-3796/

~40–60 MW/m^2 for the next generation ST-based Fusion Nuclear Science Facility (FNSF) [8], Pilot Plant [9], and a 1 GW-electric-class DEMO/Power Plant with the device size of ITER. In addition, there are serious concerns over potential damage to the PFCs by the very high transient heat fluxes accompanying ELMs and other uncontrolled events. Application of lithium (Li) in the NSTX spherical tokamak resulted in improved H-mode confinement, H-mode power threshold reduction, and ELM mitigation while maintaining essentially Li-free core plasma operation even during H-modes [10–21]. A particularly important and relevant observation from the NSTX liquid lithium divertor (LLD) experiment for the present paper is the divertor heat flux reduction accompanying the Li coating of divertor surfaces in NSTX [22]. The measurements showed a ~50% reduction in peak heat load on the divertor strike point surfaces with only a modest amount of Li (~300 mg) evaporation prior to the discharge compared to 150 mg evaporation. It is estimated that <10% of the evaporated Li is deposited over the LLD surfaces. The heat flux reduction is accompanied by an increase in the localized radiation measured by bolometers from the region above the inner and outer strike points. Motivated by this observation, a liquid lithium (LL) based radiative divertor concept termed RLLD (radiative liquid lithium divertor), has been proposed [1]. For those not familiar with the RLLD concept, it is reviewed briefly in Section 2. In Section 3, the motivation for the active Li radiation based divertor concept is described. In this paper, we examine the case of active Li injection upstream to the divertor plate, but within the divertor chamber near the divertor throat. The injected Li ionizes quickly and radiates as it flows toward the divertor plate. We term this active version of the radiative LL divertor the ARLLD. In Section 4, a model calculation for ARLLD is described. The model predicts significant reduction in the heat flux to the divertor by non-coronal equilibrium Li radiation with a modest amount of Li injection. Encouragingly, even for an ITER-sized 1 GW-electric fusion power plant, the calculated required Li evaporation rate is quite modest, i.e., ~a few mol/s. In Section 5, we discuss the ARLLD and RLLD concepts under reactor conditions. In Section 6, conclusions and discussion are given.

2. A review of radiative liquid lithium divertor (RLLD)

To briefly review the concept, the RLLD is placed at the bottom of the reactor chamber for obvious reasons from the LL handling point of view, and also to capture any impurity particles including dust generated within the reactor chamber [23] as illustrated in Fig. 1. A simplified schematic of the RLLD is shown in Fig. 2, noting that the actual RLLD shape should follow the contour of an outer divertor leg. The LL is introduced at the upper part of the RLLD at multiple toroidal locations, and it gradually flows down the RLLD side wall as a thin film via gravity and capillary action. The thin LL film thus formed should provide very effective pumping (or entrapment) of the working gas, impurities, and dust generated within the reactor chamber. The RLLD chamber being of the lowest temperature in the reactor chamber together with the usual divertor action, should facilitate the pumping of the entire reactor chamber. The RLLD chamber wall temperature can be in the 250–450 °C range, which is significantly lower than that envisioned for the fusion reactor first wall. The LL flowing down the divertor side wall accumulates at the bottom of RLLD where the divertor strike point is placed. By placing the LL surface in the path of the divertor strike point, the LL is evaporated from the surface through sputtering, evaporation, and chemical processes [24]. The evaporated Li is quickly ionized by the plasma and the ionized Li ions can radiate strongly, reducing the heat flux to the divertor strike point surfaces and protecting the substrate material.

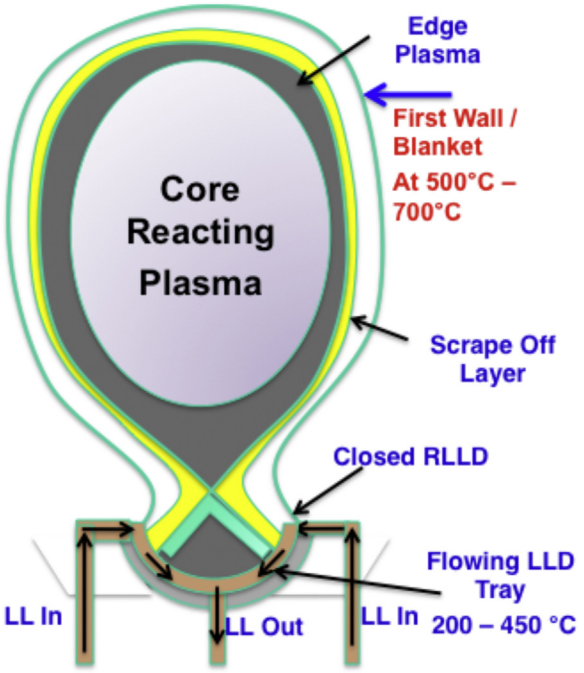

Fig. 1. A possible RLLD configuration in a fusion power plant. (a) RLLD is envisioned to be placed at the bottom of the reactor chamber to capture LL, dust, and other solid impurities.

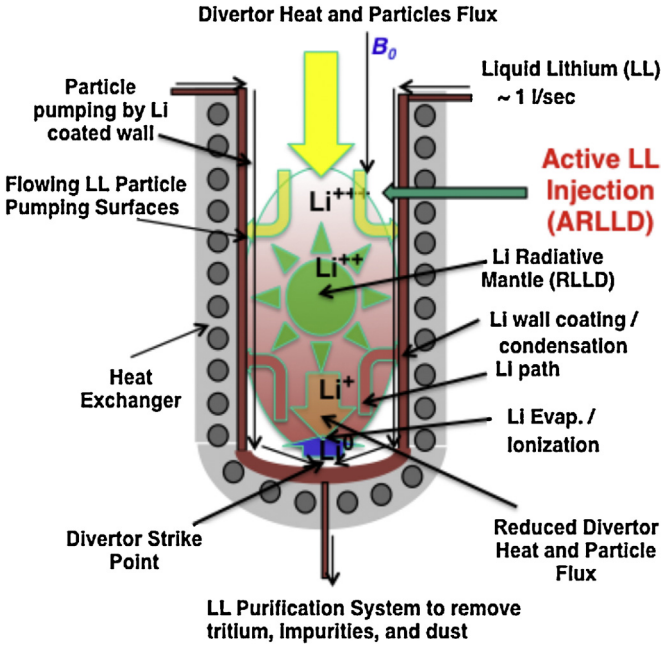

Fig. 2. A simplified schematic of RLLD chamber. The LL flows down along the side wall to provide pumping, and the thicker LL layer at the bottom provides radiative Li source for heat flux reduction and divertor substrate protection. A new feature is the active LL injection from the side wall.

3. Motivation for active radiative liquid lithium divertor (ARLLD)

The motivation for LL utilization for divetor heat flux mitigation can be seen in Fig. 3. The figure depicts various possible protective functions LL can perform for divertor PFCs. Perhaps the last line of defense is the LL evaporation from the LLD tray. Through evaporation, Li can carry some heat away from the material surfaces

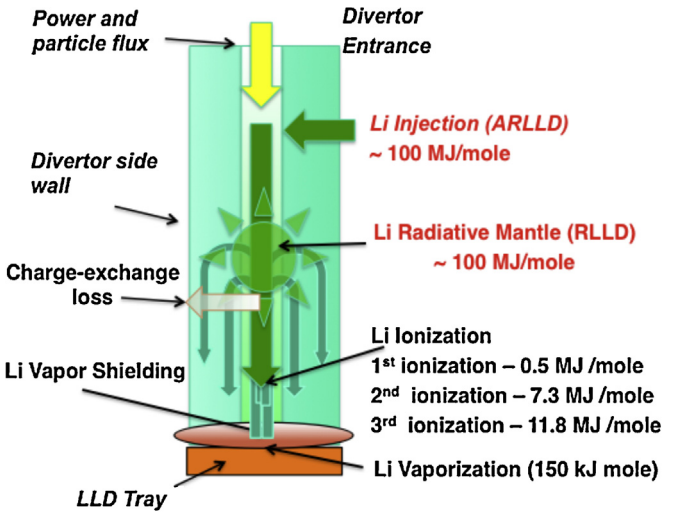

Fig. 3. Lithium–plasma interactions in the RLLD/ARLLD divertor configurations.

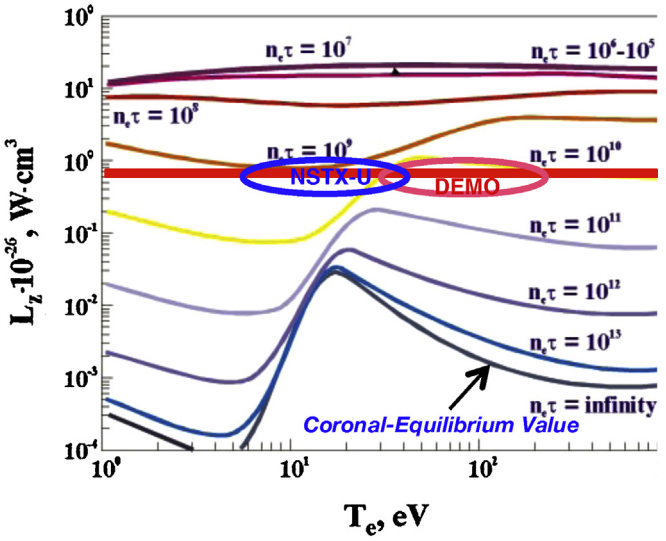

Fig. 4. The Li non-equilibrium and coronal radiation ($n_e\tau$ = infinity) power per one atom and one electron as a function of electron temperature and 'non-stationary parameter $n_e\tau$'.

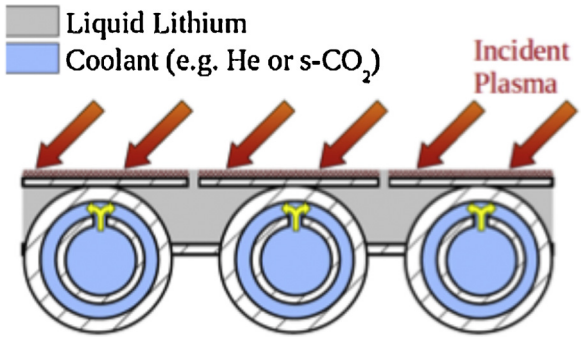

Fig. 5. Conceptual diagram for an actively-cooled, actively-wetted LL PFC.

analogous to the latent heat effect. The evaporated Li could form a Li vapor cloud in front of the divertor surface and provide some additional protective function [25]. We note that there is a divertor concept utilizing the evaporative energy to handle the divertor heat flux [26]. As the lithium enters the plasma along field line, it can ionize up to three times. As shown in the figure, one may note that the amount of energy it takes to ionize Li ions can be quite large (~20 MJ/mol) for full ionization compared to only 150 kJ/mol for vaporization. However, one may note that both vaporization and ionization processes do not actually remove the energy from the plasma, and the energy can be re-deposited back onto the divertor plate. Possible benefits of evaporation and ionization are spreading of the transient heat flux via the radial and temporal spreading of the heat flux through axial and radial diffusions as depicted in Fig. 3. There are also charge-exchange processes which can take some energy away from the plasma to the surrounding divertor wall. The energy transported per Li ion due to charge exchange is on the order of the Li ion temperature, which is non-negligible but likely to be not significant. Since the charge exchange processes may occur more preferentially in the recycling region near the divertor plate, the solid angle available to spread the heat throughout the divertor chamber maybe also limited to about a little more than 50%. The non-coronal equilibrium radiative heat dissipation has the potential of radiating a large amount of heat, estimated to be ~100 MJ/mol (or ~1 keV equivalent per lithium atom as was first pointed out in Ref. [27]), i.e., nearly three orders of magnitude larger than through the evaporative process. Indeed, the lithium radiation level of ~0.8–1 keV per lithium atom was recently reported in an experiment in the tokamak T11M [28]. This enhanced non-coronal radiation has been suggested previously through model calculations [27,29,30]. An example of such a calculation (from Fig. 16 of Ref. [30]) is shown in Fig. 4, where the radiation intensity per Li ion and electron is plotted as a function of electron temperature for various values of $n_e\tau$, where n_e is the electron density and τ is the Li ion particle confinement time. The coronal equilibrium is when $n_e\tau$ is infinite. As can be seen in the figure, the radiation can increase significantly (by several order of magnitude) above the coronal equilibrium value for poorly confined plasmas. This is because of the fact that the Li ion is highly radiative only during the initial period of its birth in the plasma. Once it is in coronal equilibrium, its radiation level becomes low. This transient radiative process is the main mechanism by which the calculated radiation level goes up nearly linearly with the inverse of $n_e\tau$ as shown in Fig. 4. The estimated radiation level used for the present calculation is indicated by the red horizontal line, and the expected divertor plasma parameter range for NSTX and DEMO is depicted by the circles in Fig. 4. We shall check this assumption in the model calculations in Section 3. Another benefit of the radiative process is that it removes and transports energy from the plasma electrons to the surrounding wall, where the deposited heat can then be removed through a secondary heat exchanger as depicted in Fig. 2. The ARLLD concept has the advantage of inducing radiative loss well away from the divertor plate, thus having a better chance of spreading the heat more evenly throughout the divertor chamber wall. There is also an increasing realization that it may be difficult to remove high steady-state heat fluxes greater than 5–8 MW/m^2 in a reactor for tungsten-based divertor PFCs. This is required in order to keep the maximum surface temperature below 1200 °C to prevent tungsten recrystallization [5], and high thermal conducting materials such as copper cannot be used in neutron environment. Instead, a more reactor compatible ferrite-based material RAFAM (F82H), which has a relatively narrow operating temperature range, is envisioned be used. Also for liquid-metal-based PFCs, there is a design study being performed to see how efficiently one can remove the heat from the liquid metal PFC surface. One concept is shown in Fig. 5, where the heat exchanger utilizes the so-called T-tube concept designed to efficiently cool the PFC sides [31]. Even with such an advanced heat exchanger configuration, the surface temperature rise can be significant, and perhaps 5 MW/m^2 maybe more realistic if we were to limit the surface (liquid) temperature rise to the 450 °C range [32]. The main aim of the present paper is therefore to

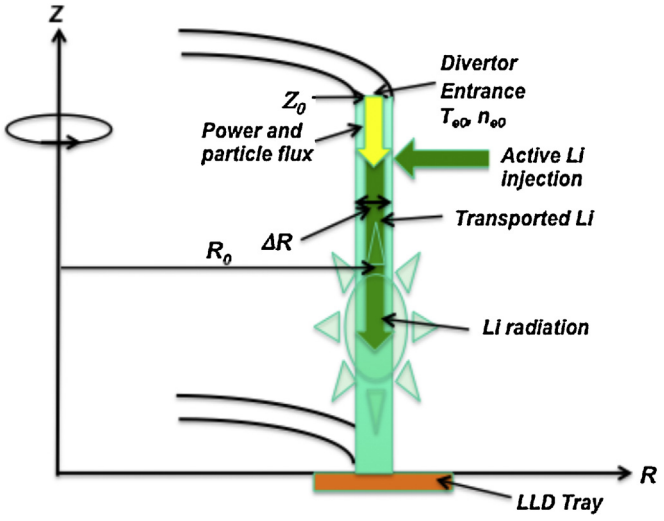

Fig. 6. A schematic of ARLLD modeling geometry.

explore the possibility of reducing the peak divertor PFC heat flux to a safe and manageable level of $\leq$5 MW/m^2, utilizing the active radiative liquid lithium divertor concept (ARLLD).

4. Model calculation of active radiative liquid lithium divertor concept

In this paper, we extend the previous model calculations for the RLLD [1] to an actively Li injected case (ARLLD). This was to estimate the effect of Li radiation on the divertor heat flux when Li is injected at the upstream region of the divertor as shown in Fig. 6. As with the previously reported case of the RLLD, to elucidate the Li radiative cooling effect, we choose a simple cylindrical shell geometry. Its radius is the divertor strike position radial position R_0, with the shell width to be an effective divertor strike point radial width ΔR and the vertical height Z_0 representing a nominal divertor vertical length as shown in Fig. 6. In this model, the magnetic field and its pitch is assumed to be constant (where the toroidal displacement $R_0\Delta\phi$ is 20 times the vertical displacement ΔZ) and, therefore, there is no flux expansion or other geometric effects within the divertor chamber. The divertor vertical region is divided into a number of cells (typically 23) and, within each cell, the plasma parameter changes due to the Li radiation are calculated using the conduction limited two-point model [33]. The Li radiated power per plasma volume is $P_{\rm Li} = I_{\rm Li} \times n_e \times n_{\rm Li}$. Here the radiation causes the volumetric heat loss $q_{\rm rad} = f_{power} \times q_0$, where q_0 is the incident heat flux into the cell. The force balance constraint within the cell leads to the reduction in the electron temperature in the cell of $\Delta T_{e0}/T_{e0} = 1 - (1 - f_{power})^2$, where T_{e0} is the electron temperature at the entrance of the cell. This model is a linear calculation and therefore does not describe non-linear processes such as divertor detachment and plasma sheath effects. The plasma parameters at the divertor entrance are assumed to be the MPTS (multi-point Thomson scattering) temperature and density measured at the plasma mid-plane with $T_i = T_e$. In this calculation, the Li is deposited at the 20th cell (where the 23rd cell is the divertor entrance), simulating an upstream injection not far from the divertor entrance. The deposited Li is assumed to be ionized with an average charge of +2, or each injected Li atom contributes 2 electrons. Therefore, the injected Li initially has a dilution effect in the 20th cell, which accordingly increases the electron density and decreases the electron temperature. The deposited Li is then assumed to flow toward the divertor plate with a velocity of $V_D \sim Cs/2.0$, which is consistent with an experimentally motivated divertor particle

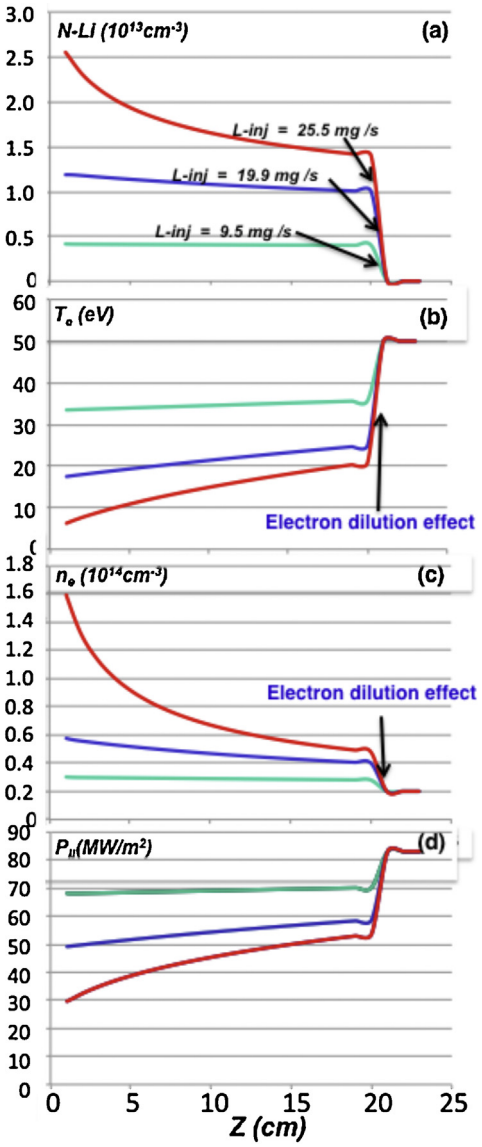

Fig. 7. Calculated divertor heat flux reduction due to Li radiation with NSTX ARLLD parameters. (a) Li particle densities for various Li injection rates as labeled as a function of axial divertor distance. (b) Electron temperature profile, (c) parallel power flux and (d) electron density profile for the corresponding Li density profiles. At the divertor throat (Z = 23 cm), T_e = 50 eV and $n_e = 2 \times 10^{13}$ cm^{-3} were used in the model.

transport model [34]. If we assume τ = 200 μs and $n_e \sim 10^{13}$ cm^{-3} or $n_e\ \tau \sim 2 \times 10^9$, from Fig. 4, one obtains $I_{\rm Li}$ (Li radiated power per one Li ion and one electron) ~0.5–1 × 10^{-26} W cm^3 for a relatively wide range of plasma temperatures. We will therefore use $I_{\rm Li} \sim 5 \times 10^{-27}$ W cm^3 for this modeling calculation. We should note that the amount of Li injection required is relatively insensitive to the assumption of $V_D \sim Cs/2.0$. If the V_D is larger or smaller than $Cs/2.0$, the Li density would be accordingly smaller or larger since $n_{\rm Li} \propto$ Li-$inj/V_D \propto$ Li-$injx\ \tau$. But we should then note that since $P_{\rm Li} \propto I_{\rm Li}$ $n_{\rm Li} \propto I_{\rm Li}$ Li-$injx\ \tau$ and $I_{\rm Li} \propto 1/\tau$ we obtain $P_{\rm Li} \propto$ Li-inj. Therefore, the present model is relatively insensitive to the assumed divertor particle flow velocity.

For the NSTX parameters, we assume R_0 = 75 cm, ΔR = 3 cm and Z_0 = 23 cm for three levels of Li particle injection rates. The resulting Li density profile is shown in Fig. 7(a) for a given Li injection rate as labeled. As shown in Fig. 7(b), the electron temperature drops at the injection cell due to the electron dilution (density increase) by the Li injection as shown in Fig. 7(d). In this calculation, no credit

was given to the Li ionization energy since the process itself does not reduce the energy content of the plasma. As noted above, the injected Li is then transported toward the divertor plate ($Z = 0$) with a local drift speed of $Cs/2.0$. The two-point model is solved in each cell as described above with Li radiative loss. As shown in Fig. 7(c), Li radiative cooling can reduce the diverter heat flux significantly (by $\sim\times 3$) with a Li injection rate of only 26 mg/s. The corresponding density profiles are shown in Fig. 7(d), which go up toward the divertor plate as T_e is decreased due to radiation cooling, essentially preserving the parallel electron pressure. In this model, the Li particle confinement can be estimated relatively easily since it is determined by the transit time between the injection point and the divertor plate. For the most radiative case, we obtain $\tau \sim 200\,\mu$s from this model calculation, which is consistent with the assumed NSTX range of $n_e\tau$ shown in Fig. 4.

A similar estimate for an ITER-size fusion power plant (DEMO) with $R_0 = 6$ m, $\Delta R = 10$ cm, and $Z_0 = 132$ cm is shown in Fig. 8. The Li density profiles for the indicated Li injection rate, the corresponding electron temperature, parallel heat flux, and electron density profiles are shown in Fig. 8(a–d), respectively. The amount of Li injection needed to reduce the divertor heat flux is naturally much larger than in NSTX due to larger divertor size and higher heat flux, but the injected rate is still quite modest, i.e., on the order of ~mol/s. In this model, the estimated Li particle confinement time is about 600 μs, which is consistent with the assumed DEMO range of $n_e\tau$ shown in Fig. 4. Here we assumed the divertor heat flux radial channel width of 10 cm for the present power plant model calculation. In a 2 GW fusion power plant (~1 GW-electric), even assuming that only 25% of the plasma heating power of 500 MW (i.e., 400 MW of alpha power + 100 MW of auxiliary power), the 10 cm divertor heat flux channel width would still give a rather high heat flux of 35 MW/m^2. While the heat flux width is not accurately predictable at the present time, we should note that the amount of required Li injection rate is relatively insensitive to the assumption of the divertor heat flux radial width. The radiated power is linearly proportional to the lithium ion density and the required lithium ion density would be inversely proportional to the divertor power flow channel width, so that the total number of lithium ions required would remain relatively insensitive to the channel width. Finally, the present ARLLD is particularly useful for heat flux mitigation of transient events such as ELMs. For example, in an ITER-scale tokamak power plant, only a modest amount (~1 cc) of LL is estimated to be needed with the ARLLD to radiate the expected heat pulse of ~10 MJ for an exceptionally large ELM event. As discussed in the next section, the ARLLD response time should be sufficiently rapid to prevent damage to the divertor PFCs.

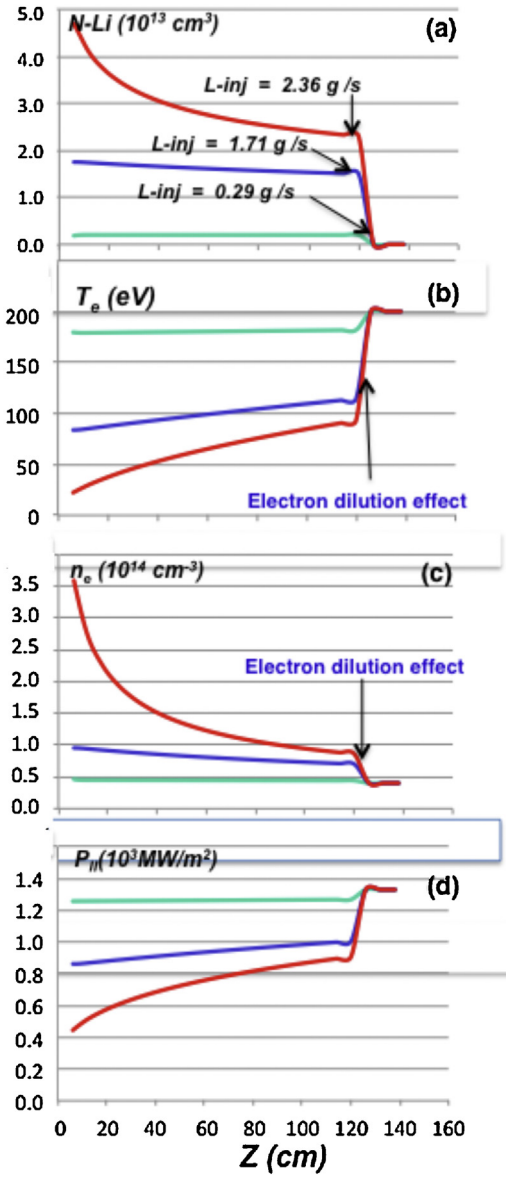

Fig. 8. Calculated divertor heat flux reduction due to Li radiation for ITER sized power plant (1 GW-e) ARLLD parameters. (a) Li particle densities for various Li injection rates as labeled as a function of axial divertor distance. (b) Electron temperature profile, (c) parallel power flux and (d) electron density profile for the corresponding Li density profiles. At the divertor throat ($Z = 138$ cm), $T_e = 200$ eV and $n_e = 4 \times 10^{13}$ cm^{-3} were used in the model.

5. RLLD and ARLLD concepts for a reactor divertor

The use of LL for a fusion reactor was motivated because of its ability to reduce edge collisionality, which produces many benefits for plasma performance. Another important property of Li is the way it does not contaminate the core plasma, as demonstrated in NSTX H-mode plasmas. Particle fuel dilution can lead to a reduction in fusion power generation even though core radiative loss are expected to be small for low Z particles such as lithium. Through NSTX experiments and related modeling, however, the Li applied in the divertor region is shown to be mainly confined within the divertor region [35].

For the ARLLD, we note the ability to provide feed back control for most transient events. Active Li injection from the divertor sidewall has the advantage of a relatively narrow divertor plasma channel (short radial travel distance) for Li delivery. The Li therefore can be delivered to the plasma quite rapidly, i.e., ~1 ms. Since the particle confinement time of injected Li is estimated to be $\leq$1 ms even for DEMO parameters, the ARLLD overall response time maybe only $\leq$a few msec which should be fast enough to protect the divertor PFCs from transient events. This is because the divertor PFC surface itself (e.g., see Figs. 3 and 6) should have a sufficient Li reservoir to tolerate a high heat flux for a short duration i.e., ~a few ms. In terms of actual Li injection, it can be a solid Li-based injector as demonstrated in NSTX [36] and EAST [37] Noting the inherently hot reactor environment, which should exceed the Li melting temperature of 180 °C, a LL-based system [38] might be more practical. One can envision a Li "spray" system which can inject LL from the divertor sidewall (see Fig. 9). Since the reactor first wall temperature is well above the Li melting temperature, it is probably realistic to assume the LL-based injector to be employed for the ARLLD reactor application.

In the previous lithium symposiums [39,40], the following specific technical issues for Li reactor applications were considered: (1)

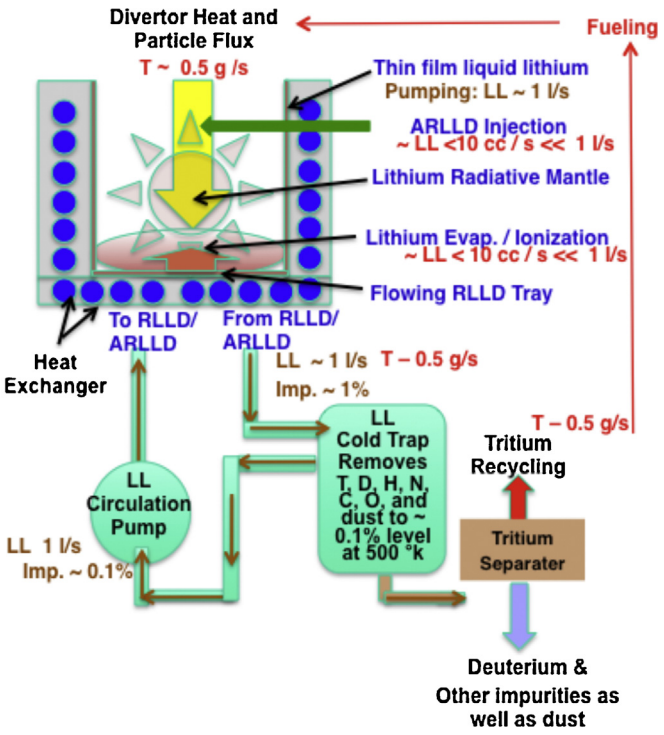

Fig. 9. A schematic for the LL purification loop for ARLLD/RLLD in a power plant.

handling high divertor heat flux, (2) removal of deuterium, tritium, and impurities from LL, (3) removal of high steady-state heat flux from divertor, (4) flowing of LL in magnetic fields, (5) longer term corrosion of internal components by LL, (6) safety of flowing LL, and (7) compatibility of LL with a hot reactor first wall. The divertor heat flux handing potential of the RLLD was already addressed in a previous reference [1] and for the ARRD, it was considered in this paper. Removal of deuterium, tritium, and impurities from LL (issue 2) was discussed previously [1], where a modest LL circulating loop of ~1.l/s is envisioned. An illustration of a LL circulation loop is also shown in Fig. 9. This level of LL circulation ensures timely removal of generated impurities, including tritium, while keeping the LL purity to be sufficient for smooth LL flow. It should be noted that 1.l/s is much larger than the ~10 cc/s (or ~1% of the LL) required to reduce the heat flux via the RLLD and ARLLD. Most of the circulating LL (~99%) can be therefore employed to coat the divertor side wall to provide sufficient pumping for the reactor system. The circulating LL system can also remove dust generated in the reactor chamber which if unchecked can lead to serious tritium inventory and reactor safety issues. We should note that a similar LL purification loop has been developed for the International Fusion Materials Irradiation Facility (IFMIF) related facilities [41]. We envision the ARLLD/RLLD LL purification loop for a power plant to have a 1000 l capacity, which is an order of magnitude smaller than that of IFMIF [1]. The LL purification loop, while technically challenging, can solve several important steady-state reactor technology issues including dust removal, minimizing tritium inventory, and providing fresh lithium for divertor pumping and heat flux mitigation with the ARLLD/RLLD. For the third issue regarding removal of high steady-state heat flux from the divertor, the RLLD and ARLLD address this, since the divertor heat load is dispersed over the large divertor wall surfaces through radiation, and the divertor heat load can be removed through secondary divertor structures with heat exchangers (as illustrated in Fig. 2.) Regarding the fourth issue of flowing of LL in magnetic fields, because of the relatively low circulating LL volume (~1.l/s), the required power for circulation is modest. In addition, the RLLD concept relies mainly on the slow LL flow via gravity and capillary action along the RLLD wall so that the magnetic field induced forces on LL should be negligible. Issues 5 and 6 concerning longer term corrosion and safety issues are well-defined materials science and safety engineering issues. The relatively low operating temperature range of the RLLD and its associated LL loop system should be advantageous from the corrosion and safety point of view. The low operating temperature also makes available broader choices of iron-based alloy materials which might be more practical to employ as a divertor-LL substrate material that is compatible with a reactor environment. It should be also noted that those engineering issues such as 5 and 6 are being addressed in the R&D activities for IFMIF [41] and fusion blanket module development. Finally the compatibility of the RLLD with a hot reactor first wall (issue 7) was resolved with lower temperature RLLD operation as previously addressed in Ref. [1].

6. Conclusions and discussion

The application of Li coatings on divertor PFCs in NSTX has produced significant improvements in H-mode plasma confinement and performance. It is also noted that even with significant application of Li on PFCs, very little contamination (<0.05%) of Li in the main fusion plasma core was observed even in H-mode plasmas. An important observation in NSTX particularly relevant for the present paper is that the application of modest Li coatings on divertor surfaces has resulted in ~50% reduction in the peak divertor heat flux. Based on the NSTX Li experimental results, we proposed a radiative cooling based LL divertor concept (RLLD) previously [1], and in this paper we introduced an actively controlled radiative LL divertor concept (ARRD). Because of the low melting temperature of ~180 °C, Li naturally exists as liquid in a fusion reactor environment, so it is a practical liquid metal to be employed in a loop system to bring tritium and impurities out of the vacuum vessel. The RLLD/ARLLD chamber being at the lowest temperature in the reactor chamber should facilitate pumping and impurity/dust removal action for the entire reactor chamber. The present RLLD/ARLLD concept is similar in philosophy to other radiative divetor concepts. However, the present Li-based divertor has a promise for improving plasma confinement and performance via low edge recycling as observed in NSTX, compared to the confinement degradation often observed with the conventional high recycling radiative divertor approach. The physics of low and high recycling divertor approaches certainly merits further study. The lack of core dilution by Li is also another important consideration for utilizing Li for this application. Noting the challenges of developing PFCs which can actually handle a steady-state heat flux of >5 MW/m^2 for both solid and liquid-based designs, the present RLLD/ARLLD approach is intended to reduce the divertor heat flux to an acceptable level before reaching the divertor PFC surfaces. One additional advantage of LL-based PFCs over tungsten-based PFCs is that LL can provide additional protection for the PFC solid substrate through evaporation, ionization, and radiation for transient high heat flux events such as ELMs. The NSTX-U facility, with reactor relevant heat fluxes [42–44], could provide physics data for the RLLD/ARLLD. It should be emphasized that the present RLLD/ARLLD concepts should work well with other innovative divertor concepts designed to mitigate divertor heat flux effects through flux expansion, such as the “snow flake” [45], “x” [46], and “super-x” divertor configurations [47]. One possible disadvantage of flux expansion concepts is that it would require extra poloidal field coil(s) near the divetor region, which may be challenging to implement in a reactor environment. The RLLD/ARLLD concepts therefore could offer additional flexibility by reducing the divertor heat flux to a safe level for both steady-state and transient heat loads in any given divertor configuration. Application of the ARLLD concept might be

suitable for protecting tungsten-based solid divertor PFC surfaces, such as the ones envisioned for ITER, from excessive heat flux since the amount of Li introduced into the vessel is relatively modest. In summary, an active radiative mantle-based LL divertor solution (ARLLD) provides added flexibility and an additional layer of protection to the previously proposed RLLD concept. This could lead to a practical solution to the highly challenging divertor heat handling issues confronting magnetic fusion reactors, while simultaneously improving the reactor performance.

Acknowledgement

This work was supported by DoE Contract No. DE-AC02-09CH11466.

References

[1] M. Ono, M.A. Jaworski, R. Kaita, H.W. Kugel, J.-W. Ahn, J.P. Allain, et al., Nucl. Fusion 53 (2013) 113030.
[2] Magnetic Fusion Energy Science Research Needs Workshop report, June 2009, http://burningplasma.org/web/ReNeW/ReNeW.report.web2.pdf
[3] ITER, Physics basis expert groups on confinement and transport and confinement modelling and database. ITER physics basis editors, Nucl. Fusion 39 (1999) 2175.
[4] R.E. Nygren, R. Raffray, D. Whyte, M.A. Urickson, M. Baldwin, L.L. Snead, J. Nucl. Mater. 417 (2011) 451.
[5] K. Tobita, S. Nishio, M. Enoeda, H. Kawashima, G. Kurita, H. Tanigawa, et al., Nucl. Fusion 49 (2009) 075029.
[6] E. Visca, P. Agostini, F. Crescenzi, A. Malavasi, A. Pizzuto, P. Rossi, et al., Fusion Eng. Des 87 (2012) 941.
[7] X.R. Wang, S. Malang, M.S. Tillack, J. Burke, Fusion Eng. Des. 87 (2012) 732.
[8] Y-K.M. Peng, T.W. Burgess, A.J. Carroll, C.L. Neumeyer, J.M. Canik, M.J. Cole, et al., Fusion Sci. Technol. 56 (2009) 957.
[9] J.E. Menard, L. Bromberg, T. Brown, T. Burgess, D. Dix, L. El-Guebaly, et al., Nucl. Fusion 52 (2012) 083015.
[10] M. Ono, S.M. Kaye, Y.-K.M. Peng, G. Barnes, W. Blanchard, M.D. Carter, et al., Nucl. Fusion 40 (2000) 557.
[11] H.W. Kugel, M.G. Bell, J.-W. Ahn, J.P. Allain, R. Bell, J. Boedo, et al., Phys. Plasmas 15 (2008) 056118.
[12] H.W. Kugel, J.P. Allain, M.G. Bell, R.E. Bell, A. Diallo, R. Ellis, et al., Fusion Eng. Des. 87 (2012) 1724.
[13] M.G. Bell, H.W. Kugel, R. Kaita, L.E. Zakharov, H. Schneider, B.P. LeBlanc, et al., Plasma Phys. Control. Fus. 51 (2009) 124054.
[14] R. Maingi, T.H. Osborne, B.P. LeBlanc, R.E. Bell, J. Manickam, P.B. Snyder, et al., Phys. Rev. Lett. 103 (2009) 075001.
[15] S.M. Kaye, R. Maingi, D. Battaglia, R.E. Bell, C.S. Chang, J. Hosea, et al., Nucl. Fusion 52 (2011) 1823.
[16] S.M. Kaye, S. Gerhardt, W. Guttenfelder, R. Maingi, R.E. Bell, A. Diallo, et al., Nucl. Fusion 53 (2013) 063005.
[17] R. Maingi, D.P. Boyle, J.M. Canik, S.M. Kaye, C.H. Skinner, J.P. Allain, et al., Nucl. Fusion 51 (2012) 083001.
[18] R. Maingi, R.E. Bell, J.M. Canik, S.P. Gerhardt, S.M. Kaye, B.P. LeBlanc, et al., Phys. Rev. Lett. 105 (2010) 135004.
[19] M. Podesta, R.E. Bell, A. Bortolon, N.A. Crocker, D.S. Darrow, A. Diallo, et al., Nucl. Fusion 52 (2012) 033008.
[20] F. Scotti, V.A. Soukhanovskii, R.E. Bell, S. Gerhardt, W. Guttenfelder, S. Kaye, et al., Nucl. Fusion 53 (2013) 083001.
[21] M. Ono, M.G. Bell, R.E. Bell, R. Kaita, H.W. Kugel, B.P. LeBlanc, et al., Fusion Eng. Des. 85 (2010) 882.
[22] T.K. Gray, J.M. Canik, R. Maingi, A.G. McLean, J.-W. Ahn, M.A. Jaworski, et al., The effects of increasing lithium deposition on the power exhaust channel in NSTX, Nucl. Fusion 54 (2014), 023001.
[23] C.H. Skinner, B. Rais, A.L. Roquemore, H.W. Kugel, R. Marsala, T. Provost, Rev. Sci. Instrum. 81 (2010) 10E102.
[24] R.P. Doerner, M.J. Baldwin, R.W. Conn, A.A. Grossman, S.C. Luckhardt, R. Seraydarian, et al., J. Nucl. Mater. 290–293 (2001) 166.
[25] T. Abrams, M.A. Jaworski, R. Kaita, D.P. Stotler, G. De Temmerman, T.W. Morgan, et al., Fusion Eng. Des (2014), accepted for publication.
[26] Y. Nagayama et al., *Fusion Eng. Des*. 84 1380.
[27] T.D. Rognlien, M.E. Rensink, Phys. Plasmas 9 (2002) 2120.
[28] S.V. Mirnov, A.M. Belov, N.T. Djigailo, A.N. Kostina, V.B. Lazarev, I.E. Lyublinski, et al., J. Nucl. Mater. S224–S228 (2013) 438.
[29] V. Lazarev, E. Azizov, A. Alekseyev, A. Belov, S. Mirnov, V. Petrov, et al., 1999 26th EPS Conf. on Controlled Fusion and Plasma Physics (Maastricht, The Netherlands, 14–18 June) (ECA) 231 (1999) 845.
[30] V.A. Evtikhin, I.E. Lyublinski, A.V. Vertkov, S.V. Mirnov, V.B. Lazarev, N.P. Petrova, et al., Plasma Phys. Control. Fusion 44 (2002) 955.
[31] M. Nieto, D.N. Ruzic, W. Olczak, R. Stubbers, J. Nucl. Mater. 350 (2006) 101.
[32] M.A. Jaworski, A. Khodak, R. Kaita, Plasma Phys. Control. Fusion (2013) (in press).
[33] P.C. Stangeby, The plasma boundary of magnetic fusion devices", IOP, Bristol, 2002.
[34] R.G. Goldstone, Nucl. Fusion 52 (2012) 013009.
[35] F. Scotti, Bull. Am. Phys. Soc. 75 (2012) 109.
[36] D.K. Mansfield, A.L. Roquemore, H. Schneider, J. Timberlake, H. Kugel, M.G. Bell, et al., Fusion Eng. Des. 85 (2010) 890.
[37] D. Mansfield, A.L. Roquemore, T. Carroll, Z. Sun, J.S. Hu, L. Zhang, et al., Nucl. Fusion 53 (2013) 113023.
[38] Andruczyk D. et al., *Fusion Eng. Des*. (submitted for publication).
[39] Y. Hirooka, G. Mazzitelli, S.V. Mirnov, M. Ono, M. Shimada, F.L. Tabares, Nucl. Fusion 50 (2010) 077001.
[40] M. Ono, Y. Hirooka, G. Mazzitelli, S.V. Mirnov, M. Shimada, F.L. Tabares, Nucl. Fusion 52 (2012) 037001.
[41] H. Kondo, T. Furukawa, Y. Hirakawa, H. Iuchi, M. Ida, J. Yagi, et al., Fusion Eng. Des. 86 (2011) 2437.
[42] J.E. Menard, S. Gerhardt, M. Bell, J. Bialek, A. Brooks, J. Canik, et al., Nucl. Fusion 52 (2012) 083015.
[43] T. Gray, R. Maingi, V.A. Soukhanovskii, J.E. Surany, J.-W. Ahn, A.G. MaLean, et al., J. Nucl. Matter 415 (2011) S360.
[44] M. Ono, M.G. Bell, R. Kaita, H.W. Kugel, J.-W. Ahn, J.P. Allain, et al., Fusion Eng. Des 87 (2011) 1770.
[45] V.A. Soukhanovskii, J.-W. Ahn, R.E. Bell, D.A. Gates, S. Gerhardt, R. Kaita, et al., Nuclear Fusion 51 (2011) 012001.
[46] M. Kotschenreuther, P.M. Valanju, S.M. Mahajan, J.C. Wiley, Phys Plasmas 14 (2007) 072502.
[47] P.M. Valanju, M. Kotschenreuther, S.M. Mahajan, J. Canik, et al., Phys. of Plasmas 16 (2009) 056110.